Broad-Spectrum Optical Turbulence Assessments from Climatological Temperature, Pressure, Humidity, and Wind

Steven T. Fiorino,* **Richard J. Bartell, Matthew J. Krizo,**
Brandon T. McClung, J. Jean Cohen, Robb M. Randall, and
Salvatore J. Cusumano

Center for Directed Energy, Air Force Institute of Technology, 2950 Hobson Way,
Wright–Patterson Air Force Base, Ohio 45433-7765

The effects of optical turbulence on high-energy laser propagation have been well documented. The optical turbulence is typically characterized using the index of refraction structure parameter, C_n^2. The value and three-dimensional variation of C_n^2 can be accurately diagnosed for the surface boundary layer (lowest 50 m of the atmosphere) from values of temperature, pressure, humidity, and wind velocity using meteorological similarity theory. Examples of such similarity theory C_n^2 calculators include the Tunick model for overland applications and the Navy Surface Layer Optical Turbulence (NSLOT) model for ocean scenarios. Both the Tunick and NSLOT models are limited in their applicability to relatively small portions of the spectrum in the visible and infrared; generally they are valid from 400 to 3,000 nm and from 7.8 to 19 μm. This study expands the valid spectral range of the Tunick C_n^2 model to 400 nm–8.6 m, continuously. This is accomplished by adapting the Tunick model for use with the Air Force Institute of Technology Center for Directed Energy's HELEEOS (High Energy Laser End-to-End Operational Simulation) and LEEDR (Laser Environmental Effects Definition and Reference) models. The derived C_n^2 values can be wavelength tuned and compared to scintillometer and radar measurements of C_n^2.

1. Introduction

For the purpose of evaluating expected directed energy weapon (DEW) system performance, the Air Force Institute of Technology (AFIT) Center for Directed Energy (CDE) has developed several modeling codes to simulate operating conditions. One of these codes, the High Energy Laser End-to-End Operational Simulation (HELEEOS),[1,10] is perhaps the first DEW simulation package to fully incorporate a correlated, probabilistic climatological database. The infusion of such realistic atmospheric effects into the simulations allows

---

HELEEOS to better assess variability/uncertainty in DEW system performance arising from spatial, spectral, and temporal variations in operating conditions. This paper highlights a newly implemented capability within HELEEOS that allows the broad-spectrum calculation of surface layer optical turbulence (C_n^2) values based on the HELEEOS climatological database.

The capability to create realistic data profiles of correlated atmospheric effects, including optical turbulence, on electromagnetic energy propagation extends far beyond DEW system performance. Thus AFIT CDE has produced a separate atmospheric effects definition and reference tool, the Laser Environmental Effects Definition and Reference, or LEEDR,[9] that allows the export of the first-principles atmospheric characterizations for other DEW simulation codes, military or Department of Defense mission planners, or even nonmilitary scientific research such as climate change impact studies.

The AFIT CDE models allow the real part of the index of refraction calculation to be coupled with the imaginary part of the refractive index by folding in absorption spectra from the 2004 HITRAN database embedded in both HELEEOS and LEEDR. This permits the C_n^2 calculations in anomalously dispersive regions of the spectrum that have previously been avoided, such as strongly absorbing water vapor regions in the terahertz portion of the spectrum. Thus the complete wavelength dependence of C_n^2 can be assessed from the ultraviolet to the radio frequencies, and C_n^2 measured at one wavelength can be applied with confidence at another. Comparisons to scintillometer and operational National Weather Service (NWS) radar data are made when possible. Comparisons to the radar data offer a unique comparison as the refractive index for the microwave energy is significantly affected by both temperature and humidity gradients.

2. LEEDR Description and Calculations

LEEDR is a fast-calculating, first-principles atmospheric characterization package. It enables the creation of vertical profiles of temperature, pressure, water vapor content, optical turbulence, and atmospheric particulates and hydrometeors as they relate to line-by-line layer extinction coefficient magnitude at wavelengths from the ultraviolet to radio frequencies. In addition to its extremely broad spectrum of consideration and correlated, probabilistic databases, LEEDR uniquely allows for a temporally and spatially varying atmospheric boundary layer in the production of its vertical profiles of data. This allows LEEDR to produce profiles of meteorological data and effects that could actually occur or have actually occurred at a particular location and time and attach the statistical likelihood of such occurrence for that time and place. This differs significantly from using "standard" atmospheric profiles (e.g., the U.S. Standard Atmosphere) in engineering analyses or simulations.

2.1. Climatological Databases

Worldwide seasonal, diurnal, and geographical spatial–temporal variation in meteorological parameters in LEEDR is organized into probability density function (PDF) databases using a variety of recently available resources to include the ExPERT[20] database, the Master Database for Optical Turbulence Research in Support of the Airborne Laser,[4] the Global Aerosol Data Set (GADS),[15] and Air Force Weather Agency numerical weather forecasting data. GADS provides aerosol constituent number densities on a 5×5 deg grid worldwide. ExPERT mapping software allows the LEEDR operator to choose from specific site or

regional surface and upper air data to characterize correlated molecular absorption, aerosol absorption, and scattering by percentile.[10] The PDF nature of the LEEDR atmospheric effects data enables realistic probabilistic outcome analyses. Integration of the Surface Marine Gridded Climatology v2.0 database and the Advanced Navy Aerosol Model (ANAM)[12] provides worldwide coverage over all ocean regions on a 1×1 deg grid. Molecular scattering is computed based on Rayleigh theory. Molecular absorption effects are computed for the top 13 absorbing species using line strength information from the HITRAN 2004 database[19] in conjunction with a community standard molecular absorption continuum code. Aerosol scattering and absorption are computed with the Wiscombe Mie model.[23]

Several optical turbulence profiles are available in LEEDR, for example, Hufnagel-Valley 5/7[14] and Clear 1.[2] The climatological C_n^2 profile is a novel feature of LEEDR and HELEEOS. It combines the extensive climatological record of the ExPERT database with the optical turbulence data of the Master Database for Optical Turbulence Research in Support of the Airborne Laser. The optical turbulence database is a direct compilation of many worldwide nighttime thermosonde campaigns. Each climatological C_n^2 profile is tailored to individual sites by distinctly referencing the optical turbulence database based on user-selected surface relative humidities. LEEDR physically correlates temperature and relative humidity percentiles to corresponding percentage values in the optical turbulence database. Within the boundary layer, LEEDR correlates the optical turbulence profiles to percentiles of relative humidity and in the free atmosphere to standard atmosphere temperature percentiles. These physical correlations to probabilistic climatology form the basis of the climatological C_n^2 profiles, a feature unique to the HELEEOS/LEEDR packages.[13] Over the first 50 m of the ocean surface, LEEDR employs the Navy Surface Layer Optical Turbulence (NSLOT)[11] model. Above the lowest 50 m, the Hufnagel-Valley 5/7 model is used to define over-ocean C_n^2 values.

LEEDR supports any user-defined wavelength from 0.40 μm to 8.6 m, with 24 specific wavelengths typically associated with laser operation available via lookup table for minimum runtime. LEEDR provides vertical profiles of atmospheric data and effects from the surface to any user-specified altitude up to 100 km. Figure 1 illustrates how LEEDR performs as a single line-by-line analysis tool across a very broad portion of the electromagnetic spectrum while concurrently considering a wide range of meteorological/atmospheric effects that can be varied realistically worldwide.

2.2. Overview of the complex index of refraction and the anomalous dispersion calculator

The complex index of refraction can be described as

$$N = n_r + i n_i, \qquad (1)$$

where N is the complex index of refraction, n_r is the real part of the index, and n_i is the imaginary part. If $n_i = 0$ and $N = n_r$, then the phase speed of the electromagnetic radiation, c', is determined by

$$c' = \frac{c}{n_r} \qquad (2)$$

where c is the speed of light in a vacuum. Thus the real part determines the phase speed, scattering, and turbulence characteristics. In air at typical temperature and pressure, n_r is approximately 1.0003. The imaginary part, n_i, is a measure of the absorptive properties
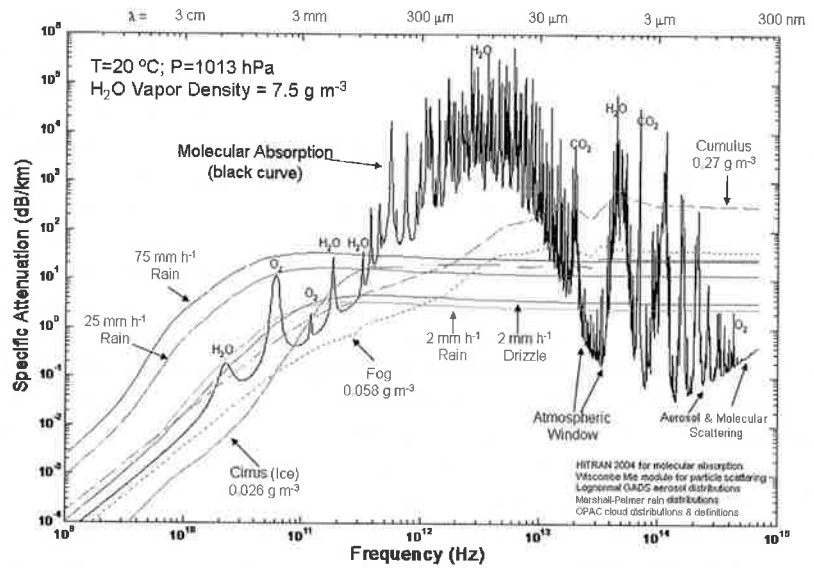
Fig. 1. Specific attenuation across wavelengths from 30 cm to ~0.4 μm. The black line is molecular absorption with some effects of continent average aerosols and molecular scattering included. Other lines represent the specific attenuation that would be added for the hydrometeor distributions shown (rain, clouds, fog).

of the medium and is sometimes called the absorption index. Both the real and imaginary parts of the index have a wavelength or frequency dependence. In the absence of strong absorption lines, the variation of the real index with wavelength is often referred to as normal dispersion. This is shown in Fig. 2 as the refractivity, $(n_r - 1) \times 10^6$, variation with wavelength using some commonly used dispersion expressions.[5,7,8]

The real and imaginary parts of the complex index can be described with the Lorentz–Lorenz relationships as outlined in Ref. 16. Mathematically these take the form of

$$k_{\tilde{v}} = \frac{4\pi n_i}{\lambda} = \frac{NS}{\pi} \frac{\alpha_N}{(\tilde{v} - \tilde{v}_0)^2 + \alpha_N^2}, \tag{3}$$

$$n_r - 1 = \frac{NS}{4\pi \tilde{v}_0} \frac{\tilde{v} - \tilde{v}_0}{(\tilde{v} - \tilde{v}_0)^2 + \alpha_N^2}, \tag{4}$$

where k_v is the monochromatic absorption coefficient (inverse length), $\tilde{v}_0$ is the wavenumber of the absorbing line (cm^{-1}), $\tilde{v}$ is the wavenumber of the calculation (cm^{-1}), λ is the wavelength, S is the line strength or intensity (cm^{-1}/molecule cm^{-1}), α_N is the line halfwidth at half-maximum (cm^{-1}/atm), and N is the molecule number density per unit volume.

Figure 3 is a schematic plot of the relationship between the imaginary and real indices and illustrates the effect of a strong absorption line on the real part of the index of refraction in air.

Notably, all the commonly used dispersion equations—such as those highlighted in Fig. 2—for the real part of the index of refraction are based on the Lorentz–Lorenz relationship, but they all apparently assume $\alpha_N = 0$. The α_N is the damping force in the Lorentz
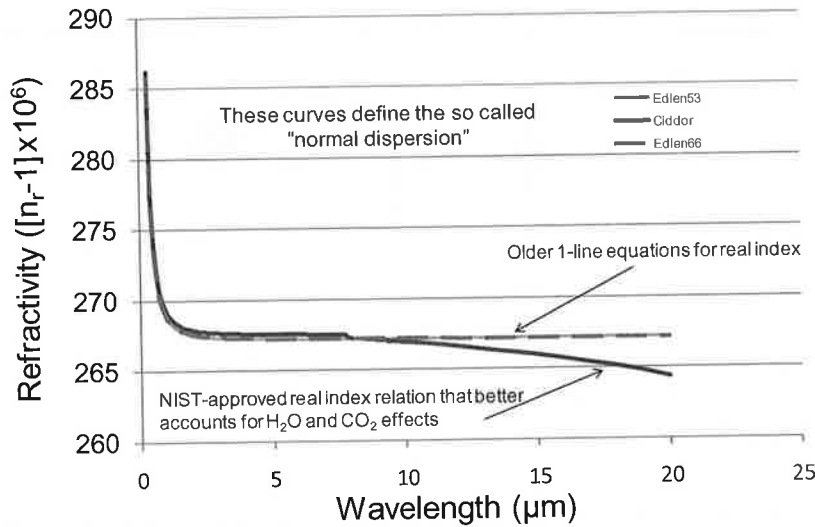
Fig. 2. Normal dispersion relationships in terms of refractivity vs. wavelength from 400 nm to 20 μm. The Edlen53[7] and Edlen66[8] formulations are very similar; the more recent Ciddor[5] equations incorporate both continuum water vapor and carbon dioxide effects. Conditions plotted are temperature 293 K, pressure 1,013 hPa, and absolute humidity 7.5 g kg^{-3}.
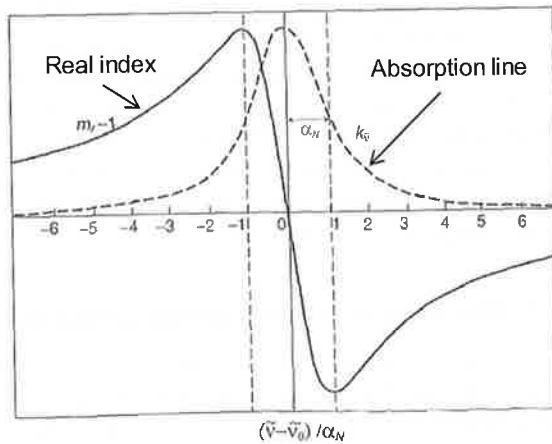

Fig. 3. Schematic after Ref. 16 of the effect of an absorption line on the real index of refraction. Note that m_r is the real index.

oscillating dipole model. This was justified by the assumption that gases are only weakly interacting with electromagnetic energy. The commonly used equations have essentially assumed relationships that account for the general "polarizability" of certain gases (e.g., water vapor and carbon dioxide), rather than the individual absorption lines, which are now well accounted for in the HITRAN database.
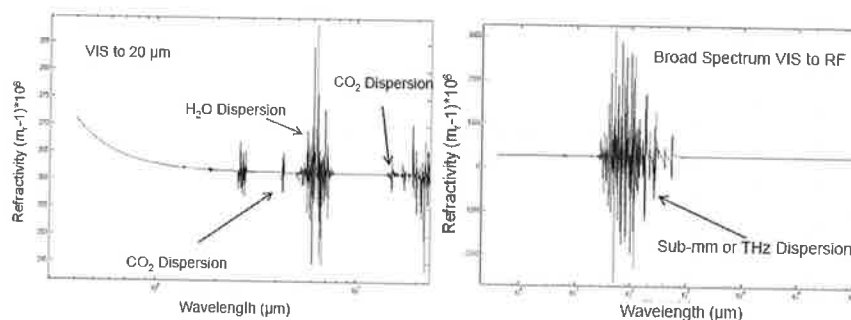
Fig. 4. Left: Real index of refraction (in refractivity units) for air 400 nm–20 μm at 294 K, 1,000 hPa, and RH = 70%. Includes anomalous dispersion effects due to strong absorption lines. Right: Same, but extended to 1-m wavelength; note that refractivity units vary from $\sim$ −2,500 to 3,000.

One of the latest additions to HELEEOS/LEEDR is an index of refraction or refractive dispersion calculator. This algorithm takes advantage of LEEDR's broad-spectrum access to the HITRAN absorption database and couples it to the Lorentz–Lorenz relationships outlined in Refs. 16 and 17 to account for anomalous dispersion at strong absorption lines. Thus refractivity can be accurately assessed at any wavelength from 400 nm to 8.6 m for any atmospheric condition. Currently, common refractivity equations are generally valid only for very limited portions of the visible, near-infrared, infrared, and microwave portions of the spectrum. The LEEDR refractivity calculator includes the increasingly important terahertz portion of the spectrum and accounts for the marked absorption features found at those wavelengths. The left-side plot in Fig. 4 illustrates LEEDR capability to calculate the refractivity for a set of conditions in the 400-nm to 20-μm region, and the broad-spectrum right-side plot clearly shows the extreme refractivity values in the terahertz or submillimeter region. Thus the HEELEOS and LEEDR climatological C_n^2 profiles, and the standard C_n^2 profiles, will be applicable with proper conversion to portions of the spectrum with refractivity conditions completely different from the "optical" spectral regions for which the C_n^2 values were originally measured.

2.3. Similarity theory and optical turbuence

Optical turbulence results in variations in the speed at which electromagnetic waves propagate.[22] What causes the speed of the electromagnetic waves to change is the propagation of the wave through different densities. In the atmosphere, the ideal gas law applies in most cases, showing that the density is dependent on the temperature, pressure, and humidity of the atmosphere. The model created herein is also dependent on the pressure and temperature. Because there are different temperatures at different layers in the atmosphere, each layer has a different density—causing the electromagnetic energy to propagate at different speeds, bending as it passes through the layers. Small-scale turbulence, or optical turbulence, causes density gradient irregularities that cause smaller scale bending of the electromagnetic energy and intensity fluctuations, or scintillation. This can be characterized with an index of refraction structure parameter, C_n^2.

Previous models of C_n^2 in the atmosphere have taken advantage of Monin–Obukhov scaling theory. This scaling theory applied different gradients to the microphysics of the

atmosphere to effectively calculate the value of C_n^2 in the boundary layer.[18] Using this type of theory, also called similarity theory, scaling constants for specific humidity, wind speed, and temperature can be calculated and then used to solve for the gradients of each. These gradients can be used to solve for the gradient of the index of refraction, which is used to calculate C_n^2.

Previous models are limited because they were applicable only to visible and near-infrared wavelengths. The overland surface layer C_n^2 model created by Tunick[22] is valid from 0.36 to 3.0 and 7.8 to 19 μm. The reason for the limited wavelength dependence is that the index of refraction equations used were valid only in that range. Rearranging the index of refraction equations to solve for refractivity, $N = (n_r - 1) \times 10^6$, the refractivity value at 19 μm was extended out to calculate the refractivity into the radio wavelengths ($\sim$8 m). This baseline (nonanomalous) extension can be seen in Fig. 4.

In addition to the wavelength extension, this model also incorporates anomalous dispersion. Anomalous dispersion is a large change in refractivity with a small change in wavelength. Anomalous dispersion occurs when the change in refractivity with wavelength is greater than zero, or $\partial n/\partial \lambda > 0$. Normal dispersion is when the opposite effects take place. Figure 4 shows a good example of anomalous dispersion in the 6–7-μm range, where there are numerous absorption lines for water vapor. Anomalous dispersion is incorporated by accessing the HITRAN database used in HELEEOS/LEEDR.

2.4. Mathematical derivation

The following derivation of the model's mathematics can be considered a top-down approach. First the equation for the index of refraction structure parameter will be presented, and then each term in the equation will be derived and explained. The equation for the index of refraction structure parameter used is given in Eq. (5)[21]:

$$C_n^2 = b \frac{K_H}{\varepsilon^{\frac{1}{3}}} \left(\frac{\partial n}{\partial z} \right)^2.$$

(5)

Here, b is a constant with a value of 3.2, K_H is the turbulent exchange coefficient for heat diffusion, and ε is the energy dissipation rate.[22] The most difficult term to derive is $\partial n/\partial z$, which is the vertical gradient of the index of refraction. With some algebra and a little calculus, $\partial n/\partial z$ can be written in terms of the refractivity. Doing so allows us to easily obtain $\partial n/\partial z$ with and without anomalous dispersion. The process of finding $\partial n/\partial z$ is outlined below. For the visible spectrum and near infrared (0.36–3 μm), the equation for the index of refraction, n_v, is

$$n_v = 1 + \left\{ M_1(\lambda) \frac{P}{T} + 4.615[M_2(\lambda) - M_1(\lambda)]Q \right\} \times 10^{-6},$$

(6)

where $M_1(\lambda)$ and $M_2(\lambda)$ are equations for the dispersion of dry air, water vapor, and carbon dioxide. These are defined as

$$M_1(\lambda) = 23.7134 + \frac{6,839.397}{130 - \sigma^2} + \frac{45.473}{38.9 - \sigma^2},$$

$$M_2(\lambda) = 64.8731 + 0.58058\sigma^2 - 0.007115\sigma^4 + 0.0008851\sigma^8, \qquad \sigma = 1/\lambda.$$

Equation (6) can be transformed as a function of specific humidity and potential temperature; while solving for refractivity, this gives

$$(n_v - 1) \times 1e6 = M_1(\lambda)\frac{P}{\theta - \phi_d(z - z_r)} + \frac{1.60948[M_2(\lambda) - M_1(\lambda)]Pq}{\theta - \phi_d(z - z_r)} = N. \qquad (7)$$

Then taking the partial derivatives of Eq. (7) with respect to potential temperature and specific humidity gives an expression for $\partial n/\partial z$ in the visible spectrum:

$$\frac{\partial n_v}{\partial z} \times 1e6 = \left\{ -M_1(\lambda)\frac{P}{T^2} - 1.60948[M_2(\lambda) - M_1(\lambda)]\frac{Pa}{T^2} \right\} \frac{\partial \theta}{\partial z}$$

$$+ \left\{ 1.60948[M_2(\lambda) - M_1(\lambda)]\frac{P}{T} \right\} \frac{\partial q}{\partial z}. \qquad (8)$$

Noting that Eq. (8) contains terms in Eq. (7), Eq. (8) can be written in terms of the refractivity:

$$\frac{\partial n_v}{\partial z} = \left\{ \left[-\frac{N}{T} \right] \frac{\partial \theta}{\partial z} + \left[N - M_1(\lambda) \times \frac{P}{T} \right] \frac{\partial q}{\partial z} \right\} \times 1e\text{-}6. \qquad (9)$$

A similar process can be followed in the infrared (IR) region (7.8–19 μm) to obtain an expression for $\partial n/\partial z$. The expression for $\partial n/\partial z$ in the IR is

$$\frac{\partial n_{ir}}{\partial z} \times 1e6 = \left[-\frac{N}{T} + 1.60948M_2(\lambda)\frac{Pq}{T^2} + 0.34875\frac{Pq}{T}[A] - 0.34875[B]\frac{Pq}{T^2} \right.$$

$$\left. -\frac{Pq0.6135\alpha^{-0.88}}{RT\quad Y^2} \right] \frac{\partial \theta}{\partial z} + \left[N - M_1(\lambda)\frac{P}{T} - 1.60948M_2(\lambda)\frac{P}{T} \right.$$

$$\left. + 0.34875[B]\frac{P}{T} \right] \frac{\partial q}{\partial z}, \qquad (10)$$

$$[A] = \frac{[-1.359\alpha^{-0.6}]}{Y} + \frac{0.5949\alpha^{-0.48}(X-1)}{Y^2}, \qquad (11)$$

$$[B] = \frac{957 - 928\alpha^{0.4}(X-1)}{1.03\alpha^{0.17} - 19.8X^3 + 8.2X^4 - 1.7X^8} + \frac{3.747e6}{12{,}499 - X^2}$$

$$= \frac{957 - 928\alpha^{0.4}(X-1)}{Y} + \frac{3.747e6}{12{,}499 - X^3}, \qquad (12)$$

$$Y = 1.03\alpha^{0.17} - 19.8X^2 + 8.2X^4 - 1.7X^8, \quad \alpha = T/273.15, \quad X = 10/\lambda. \qquad (12a)$$

Note that in both $\partial n/\partial z$ expressions, $\partial \theta/\partial z$ and $\partial q/\partial z$ are present. These can be found using similarity theory. Similarity theory defines the gradients of the potential temperature (θ), specific humidity(q), and wind speed (V):

$$\frac{\partial \theta}{\partial z} = \frac{\theta_*}{kz}\phi_H, \qquad \frac{\partial q}{\partial z} = \frac{\partial q_*}{kz}\phi_q, \qquad \frac{\partial V}{\partial z} = \frac{u_{0*}}{kz}\phi_m. \qquad (13)$$

Here k is the von Kármán's constant ($k = 0.4$), z is the height above the ground, and θ_*, q_*, u_* are the scaling constants for the potential temperature (Kelvin), specific humidity (g g^{-1}), and wind speed (m s^{-1}), respectively. The above equation can be rearranged to solve for the scaling constant, while assuming that the partial derivatives can be written as finite differences. Thus, the scaling constants become

$$\theta_* = \frac{k\Delta\theta}{\phi_H \Delta \ln z}, \qquad q_* = \frac{k\Delta q}{\phi_H \Delta \ln z}, \qquad u_* = \frac{k\Delta v}{\phi_m \Delta \ln z}. \qquad (14)$$

ϕ_H and ϕ_m are the dimensionless lapse rate and shear terms, respectively. In Eq. 14, it is assumed that ϕ_q, the dimensionless term for specific humidity, is equal to ϕ_H because the model is primarily run in the surface boundary layer, where the lapse rates for the humidity and temperature are often assumed to be nearly the same.

At this point in the analysis, it is important to decipher the stability of the two atmospheric layers. The atmosphere is stable if the potential temperature of the second layer is greater than the potential temperature of the first layer, whereas the atmosphere is unstable if reversed. With warm air at the lower level, the buoyancy of the air parcel causes the air to rise, causing turbulence. If the atmosphere is stable, then the lapse rates are defined as

$$\phi_m = \phi_H = 1 + 5\left(\frac{z}{L}\right), \tag{15}$$

$$L = \frac{1}{\phi_m} \frac{\theta_v(\Delta V)^2}{\Delta \ln zg[\Delta\theta + 0.61\theta\Delta q]}. \tag{16}$$

If the atmosphere is unstable, then these lapse rates become

$$\phi_m = \left[1 - 15\left(\frac{z}{L}\right)\right]^{-\frac{1}{4}}, \tag{17}$$

$$\phi_H = \left[1 - 15\left(\frac{z}{L}\right)\right]^{-\frac{1}{2}}, \tag{18}$$

$$L = \frac{\theta_v(\Delta V)^2}{\Delta \ln zg[\Delta\theta + 0.61\theta\Delta g]}. \tag{19}$$

When solving for the gradients of the atmosphere, it is important to note that the height of the atmosphere is the scaling height, or $z^* = \Delta z/\Delta \ln z$. At this point, all of the information has been provided to solve for $\partial n/\partial z$, and thus the other variables in Eq. (5) can be solved. The turbulent exchange coefficient for heat and the energy dissipation rate can be expressed as

$$K_H = \frac{u_* kz}{\phi_H}, \tag{20}$$

$$\varepsilon = \frac{u_*^3[\phi_m - (z/L)]}{kz}. \tag{21}$$

Then solving for all of the above and using Eq. (5), we can obtain a value for C_n^2 at the scaling height in the atmosphere. Tunick experimentally confirmed what several others have documented in Refs. 3, 24, and 25, that for an unstable atmosphere Eq. (22) applies and Eq. (23) applies for a stable atmosphere:

$$C_n^2(z) = C_n^2(z^*)\left(\frac{z}{z^*}\right)^{-\frac{4}{3}}, \tag{22}$$

$$C_n^2(z) = C_n^2(z^*)\left(\frac{z}{z^*}\right)^{-\frac{2}{3}}. \tag{23}$$

3. Model Implementation

The model implements these equations in MATLAB and obtains a vertical profile of C_n^2 in the atmosphere between two layers. To incorporate anomalous dispersion into the C_n^2
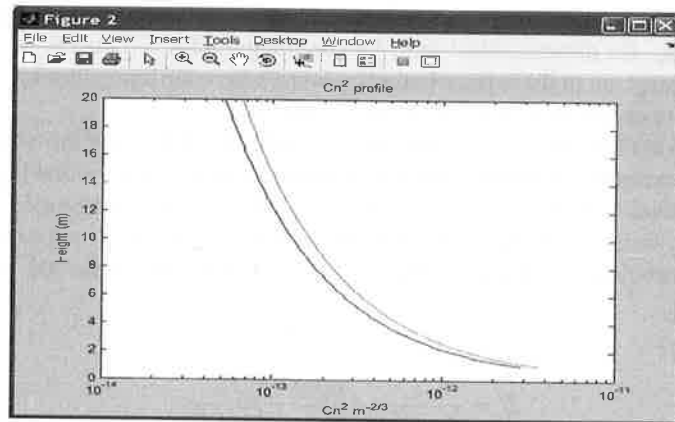
Fig. 5. Example showing the C_n^2 profile with anomalous dispersion (lighter shaded line) and without anomalous dispersion (darker shaded line) in the terahertz region at 37μm.

profile, another algorithm in HELEEOS/LEEDR is called. This algorithm uses Eq. (7) to calculate the base refractivity, then calculates the absorption data, and adds that to the base refractivity. The function would then return both the base refractivity and the absorption data so that C_n^2 profiles could be created with and without anomalous dispersion. Figure 5 shows the model output near a water vapor absorption line in the terahertz region. This shows the difference in the C_n^2 profile when anomalous dispersion is incorporated.

Two options are available to run the model. The model can be run in stand-alone mode, or it can be run in HELEEOS/LEEDR with inputs determined by the model climatological database. If the model is run stand-alone, then the graphical user interface (GUI) in Fig. 6 will pop up, allowing the user to input individual data at each level. More commonly the model will be run by HELEEOS/LEEDR, in which the climatological inputs are specified by the ExPERT database. The ExPERT database provides climatological profiles of temperature, humidity, and wind speed at different heights in the atmosphere. Looking at Fig. 6, the button panel in the bottom right-hand corner allows the user to print the C_n^2 profiles, write all of the data into a Microsoft Excel spreadsheet, or view the refractivity across a range of wavelengths.

The graph depicted on the right-hand side of Fig. 6 shows the refractivities between the two levels entered into the model. This allows the user to see the anomalous dispersion when the difference is so small that the resolution of the screen does not show it on the C_n^2 profile. When there are no absorption data, the two lines showing the C_n^2 profile with and without anomalous dispersion will be overlapping.

In HELEEOS and LEEDR, the default heights of the surface boundary layer measurement levels used are 1.5 and 11.5 m. These values are used because surface meteorological data are measured at 1.5 m, and then to keep the calculations and interpolations easy, a height difference of 10 m is used. Thus the height of the second layer is 11.5 m. When accessing the ExPERT database, the wind data and the temperature data are interpolated. The most important interpolation is with the wind data. The surface wind data in the database are assumed to be the wind data at 11.5 m. Then a linear interpolation is created to the surface, assuming that the surface wind is zero. Then from this interpolation the value of the wind speed is calculated at 1.5 m. A similar technique is used in the calculations for
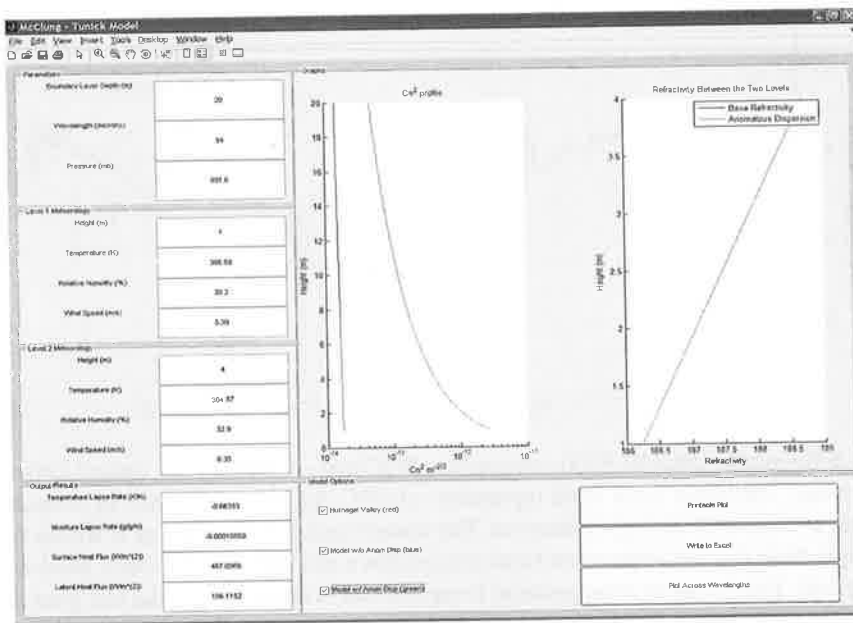
Fig. 6. The GUI used in the stand-alone model. The user will be allowed to check the Advanced Tunick option within HELEEOS and LEEDR to open the interface.

the temperatures. The surface data provided by the ExPERT database were used as the 1.5-m height. Then assuming a dry adiabatic lapse rate in the surface boundary layer, the temperature at the 11.5-m surface is calculated.

Incorporation of this "McClung–Tunick" algorithm into the HELEEOS/LEEDR model affords these models with a worldwide surface layer (lowest 50 m of the atmosphere) optical turbulence characterization capability. Previously, this surface layer optical turbulence characterization was available only over maritime regions using NSLOT. Overland areas are now covered as well.

4. Comparison Plots

Figure 7 is a comparison of optical turbulence values calculated with the McClung–Tunick model compared to C_n^2 values measured along a 700-m path with a scintillometer (BLS900). These values were obtained over a grassy field adjacent to the National Museum of the Air Force at Wright–Patterson Air Force Base (WPAFB), Ohio, on 6 November 2008. The values of C_n^2 dropped in the late afternoon before sunset due to passing high clouds that obscured the sun but left much of the rest of the sky clear. This allowed the ground to cool rapidly as if the sun had set.

In the future, radar and the index of refraction method may potentially be paired to produce a network of range-gated optical turbulence data, applicable at any wavelength. Such an optical turbulence network would have a significant impact on many applications. For example, in wireless communications, being able to stretch the maximum usable range; in imaging, being able to correct images from greater distances; and in laser weapons, affording better HEL beam propagation correction. In this theorized network, applications
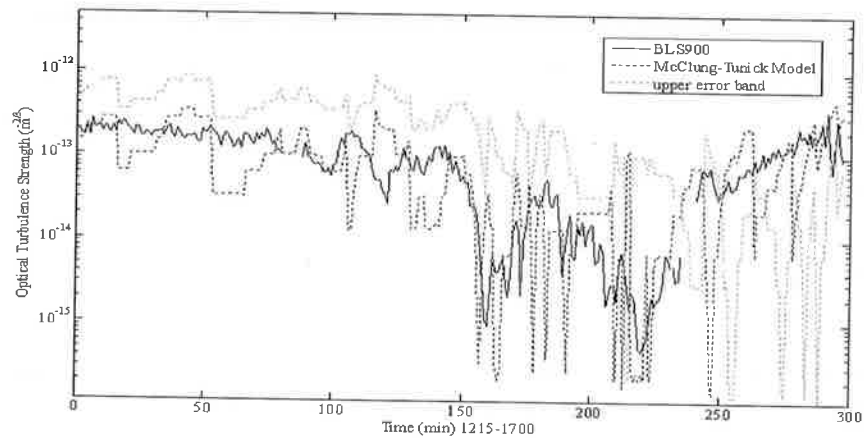
Fig. 7. 6 November 2008 BLS900 compared to McClung–Tunick model, optical turbulence versus time. The upper error band represents +0.5°C, the minimum error in temperature differences measured during calibration. The lower band is not shown as it would clutter the graph. Note that the upper error band crosses down and becomes the lower band around minute 240. This is due to a temperature inversion that is happening as the sun goes down. Dropouts in value occur when the temperature gradient is zero. Overall the model trends well around the scintillometer data, which are treated as truth data.[6]

will have available to them optical turbulence information that is real time, local, and three dimensional (3-D).[6]

As a first step in demonstrating the connection between radar and the index of refraction method, data from a 10-cm, S-band weather radar at Wilmington, Ohio, are used in conjunction with a scintillometer (BLS900) and the McClung–Tunick model. Equation (24) relates optical turbulence strength directly to radar reflectivity. Wavelength is in units of meters and dBz ranges from -26 to 0 in the radar's clear-air mode. With an estimated temperature of 5°C for the atmosphere, the resulting value for $|K_w|$ is 0.964 and $|K_w|^2$ is 0.929:

$$C_n^2 = 2.63\pi^5\lambda^{-11/3}\,|K_w|^2\,\frac{10^{(dBz/10)}}{(1,000)^6}. \tag{24}$$

Reflectivity data from the Wilmington, Ohio, NWS radar are available commercially through WeatherTap.com. Figure 8 is example Wilmington radar reflectivity from WeatherTap for tilt 1 (0.5 deg) and tilt 2 (1.5 deg). Tilt 1 gives reflectivities lower to the ground than tilt 2. The AFIT field marker is approximately 50 km away from Wilmington, Ohio. This means that the optical turbulence derived is for the atmosphere approximately 500–1,000 m above the field. In the AFIT field ring marker are nine pixels correlating to a specific reflectivity. Reflectivity is denoted by pixel color. The entire ring was averaged to provide one value for reflectivity. Black or null values were treated as -26 dBz instead of zero. This value corresponds to the minimum radar reflectivity that can be received.[6]

Figure 9 compares the scintillometer data on 6 November 2008 at WPAFB, Ohio, to clear-air radar reflectivity data obtained from the Wilmington NWS radar. Equation (24) is used to calculate the radar-derived C_n^2 values for tilt 1 and tilt 2. For the analysis shown in Fig. 9, the radar C_n^2 values are not adjusted to the scintillometer wavelength of

Fig. 8. Example of reflectivity data from WeatherTap radar analysis model.
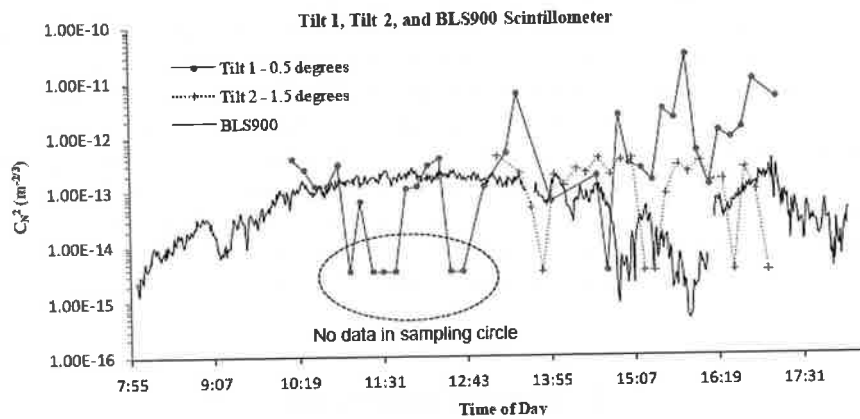

Fig. 9. 6 November 2008 BLS900 data compared to weather radar method of deriving optical turbulence. Null values of reflectivity, as seen at 11:17, cause derived turbulence values to be extremely low. This is due to AFIT's location near the edge of usability for this radar. Note that in the late afternoon tilt 1 values increase (opposite the BLS900 trend). This is due to "ground clutter" reflectivities seen when the ground and low-lying air are cooler than overlying air. Tilt 2 does not follow tilt 1's trend because it reflects off turbulence higher up.[6]

880 nm. However, a recent upgrade to the McClung–Tunick algorithm will allow for a conversion from one wavelength to another based on the input meteorological conditions. Most of the clear-air return is due to turbulence, but the tilt 1 and tilt 2 comparisons to the scintillometer data suffer somewhat from the AFIT location being on the edge of the clear-air sensitivity range of the 10-cm NWS radar. Despite the lack of returns at many of the midday times, the periods when there were returns did produce C_n^2 values near the value of the scintillometer. Correction of the C_n^2 values for the scintillometer wavelength will likely improve the comparison, as will taking scintillometer measurements nearer to the radar site. Note that the increase in the lower tilt 1 plot is due to ground clutter returns contaminating the clear-air return during the period when clouds obscured the sun and the ground cooled.

5. Summary

AFIT CDE has created within its HELEEOS and LEEDR models the capability to calculate (with iteration) the value and 3-D variation of C_n^2 within the surface boundary layer (lowest 50 m of the atmosphere) from values of temperature, pressure, humidity, and wind velocity using meteorological similarity theory. The algorithm created for this purpose utilized the overland similarity theory Tunick model as a starting point. The developed "McClung–Tunick" model expands the valid spectral range of the Tunick C_n^2 model to 400 nm–8.6 m, continuously. This has been accomplished because the AFIT CDE models allow the real part of the index of refraction calculation to be coupled with the imaginary part of the refractive index by folding in absorption spectra from the 2004 HITRAN database embedded in both HELEEOS and LEEDR. This permits the C_n^2 calculations in anomalously dispersive regions of the spectrum that have previously been avoided, such as strongly absorbing water vapor regions as the terahertz portion of the spectrum. Thus the complete wavelength dependence of C_n^2 can be assessed from the ultraviolet to the radio frequencies, and C_n^2 measured at one wavelength can be applied with confidence at another. Comparisons to scintillometer and field laser data were made and demonstrated the viability of the broad-spectrum similarity theory model and a capability to obtain optical turbulence values from operational weather radar. Operationally, the broad-spectrum McClung–Tunick algorithm affords the HELEEOS/LEEDR models the capability to produce realistic optical turbulence profiles based on climatology or real-time meteorological inputs near the ground during the day. Obtaining optical turbulence from operational weather radars allows for the creation of daytime, fair-weather 3-D optical turbulence fields in a 100-km ring around the NWS radar.

6. Acknowledgments

References

[1] Bartell, R.J., G.P. Perram, S.T. Fiorino, S.N. Long, M.J. Houle, C.A. Rice, Z.P. Manning, M.J. Krizo, D.W. Bunch, and L.E. Gravley, Proc. SPIE **5792**, 76 (2005).

[2] Beland, R.R., "Propagation through Atmospheric Optical Turbulence," in *Atmospheric Propagation of Radiation*, edited by F.G. Smith, pp. 157–232, SPIE, Bellingham, WA (1993).

[3] Ben-Yosef, N., E. Tirosh, A. Weitz, and E. Pinsky, J. Opt. Soc. Am. **69**, 1616 (1979).

[4] Bussey, A.J., J.R. Roadcap, R.R. Beland, and G.Y. Jumper, "Master Data Base for Optical Turbulence Research in Support of Airborne Laser," Air Force Research Laboratory Technical Report AFRL-VS-TR-2000-1545 (2000).

[5] Ciddor, P. E., Appl. Opt. **35**, 1566 (1996).

[6] Cohen, J.J., "Demonstration and Verification of a Broad Spectrum Anomalous Dispersion Effects Tool for Index of Refraction and Optical Turbulence Calculations," M.S. Thesis, Air Force Institute of Technology (2009).

[7] Edlen, B., J. Opt. Soc. Am. **43**, 339 (1953).

[8] Edlen, B., Metrologia **2**, 71 (1966).

[9] Fiorino, S.T., R.J. Bartell, M.J. Krizo, G.L. Caylor, K.P. Moore, T. R. Harris, and S.J. Cusumano, Proc. SPIE **6878**, 68780B (2008).

[10]Fiorino, S.T., R.J. Bartell, G.P. Perram, D.W. Bunch, L.E. Gravley, C.A. Rice, Z.P. Manning, and M.J. Krizo, J. Directed Energy 1(4), 347 (2006).

[11]Frederickson, P.A., K.L. Davidson, C.R. Zeisse, and C.S. Bendall, J. Appl. Meterol. 39, 1770 (2000).

[12]Gathman, S.G., A.M.J. van Eijk, and L.H. Cohen, Proc. SPIE 3433, 41 (1998).

[13]Gravley, L.E., S.T. Fiorino, R.J. Bartell, G.P. Perram, M.J. Krizo, and K.B. Le, J. Directed Energy 2(4), 347 (2007).

[14]Hufnagel, R.E., "Propagation through Atmospheric Turbulence," in *The Infrared Handbook*, edited by W. L. Wolfe and G. J. Zissis, Infrared Information Analysis Center, Ann Arbor, MI (1985).

[15]Koepke, P., M. Hess, I. Schult, and E.P Shettle, "Global Aerosol Data Set," MPI Meteorologie Hamburg Report No. 243 (1997).

[16]Liou, K.N., *An Introduction to Atmospheric Radiation* (2nd ed.), Academic Press, San Diego, CA (2002).

[17]Mathar, R.J., Appl. Optics 43(4), 928 (2004).

[18]Rachele, H., A. Tunick, and F. V. Hansen, J. Appl. Meteorol. 34, 1000 (1995).

[19]Rothman, L.S., C.P. Rinsland, A. Goldman, S.T. Massie, D.P. Edwards, J.M. Flaud, A. Perrin, C. Camy-Peyret, V. Dana, J.Y. Mandin, J. Schroeder, A. McCann, R.R. Gamanche, R.B. Wattson, K. Yoshino, K.V. Chance, K.W. Jucks, L.R. Brown, V. Nemtchinov, and P. Varanasi, "The HITRAN Molecular Spectroscopic Database and HAWKS (Hitran Atmospheric Workstation) 2004 edition" (2004).

[20]Squires, M.F., B.A. Bietler, S.T. Fiorino, D.L. Parks, F.W. Youkhana, and H.D. Smith, "A Method for Creating Regional and Worldwide Datasets of Extreme and Average Values," Institute of Environmental Sciences 1995 Proceedings, 41st Annual Meeting (1995).

[21]Tatarski, V.I., *The Effects of the Turbulent Atmosphere on Wave Propagation*, Israel Program for Scientific Translations, Jerusalem, Available as NTIS Technical Translation 68-50464 (1971).

[22]Tunick, A., Environmental Modeling and Software 18, 165 (2002).

[23]Wiscombe, W.J., Appl. Opt. 19(9), 1505 (1980).

[24]Wyngaard, J.C., Boundary-Layer Meteorology 9, 441 (1975).

[25]Wyngaard, J.C., and M. LeMone, J. Atmos. Sci. 37, 1573 (1980).

The Authors

Mr. Richard J. Bartell received his B.S. degree in physics from the U.S. Air Force Academy as a distinguished graduate in 1979. He received his M.S. degree from the Optical Sciences Center, University of Arizona, in 1987. He is currently a Research Physicist with the Air Force Institute of Technology's Center for Directed Energy, where he leads development of the High Energy Laser End-to-End Operational Simulation (HELEEOS) model.

Capt. J. Jean Cohen received her B.S. degree in physics from the U.S. Air Force Academy. She received her M.S. degree in applied physics from the Air Force Institute of Technology (AFIT) in 2009. This paper is an adaptation of portions of her AFIT Master's thesis. Capt. Cohen is currently assigned to the Sensors Directorate of the Air Force Research Laboratory at Wright–Patterson Air Force Base.

Dr. Salvatore J. Cusumano is the Director of the Center for Directed Energy located at the Air Force Institute of Technology (AFIT). He received his Ph.D. in control theory from the University of Illinois in 1988, an M.S.E.E. from AFIT in 1977, and a B.S.E.E. from the U.S. Air Force Academy in 1971. The Center collaborates on directed energy research topics, both high-power microwaves (HPM) and high-energy lasers (HEL), throughout the DoD community. Dr. Cusumano's research interests span his 25 years of experience in directed energy and include resonator alignment and stabilization; intracavity adaptive optics; phased arrays; telescope control, pointing, and tracking; adaptive optics; and component technology for directed energy. He holds two patents (jointly) for his work in phased arrays.

Dr. Steven T. Fiorino is a Research Assistant Professor of Atmospheric Physics at the Air Force Institute of Technology (AFIT). He has B.S. degrees in geography and meteorology from Ohio State (1987) and Florida State (1989) universities, an M.S. in atmospheric

dynamics from Ohio State (1993), and a Ph.D. in physical meteorology from Florida State (2002). His research interests include microwave remote sensing, development of weather signal processing algorithms, and atmospheric effects on military weapon systems.

Mr. Matthew J. Krizo received his M.S.E.E. from the University of Dayton in 2008 and his B.S.E.E. from Cedarville University in 2005. He is currently a Research Engineer with the Center for Directed Energy at the Air Force Institute of Technology, Wright–Patterson Air Force Base, Ohio. He is primarily responsible for software development of HELEEOS.

Lt. Brandon T. McClung received his B.S. degree in meteorology from the University of Oklahoma. He currently is a Second Lieutenant in the Air Force, where he is a forecaster for the 25th Operational Weather Squadron at Davis Monthan Air Force Base. His research contributions were primarily done at the Air Force Institute of Technology (AFIT) during an internship in the summer of 2008. He hopes to return to AFIT in future years to obtain his M.S. in applied math/physics.

Maj. Robb M. Randall is an Assistant Professor of Atmospheric Physics at the Air Force Institute of Technology (AFIT). He has a B.S. degree in meteorology from the University of Oklahoma (1995), an M.S. in meteorology from AFIT (2002), and a Ph.D. in atmospheric sciences from the University of Arizona (2007). Major Randall's research interests include understanding and characterizing the atmosphere and atmospheric effects on remote sensing.